

Rayleigh superradiance and dynamic Bragg gratings in an end-pumped Bose-Einstein condensate

A. Hilliard,* F. Kaminski, R. le Targat, C. Olausson, E.S. Polzik, and J. H. Müller

Niels Bohr Institute, Blegdamsvej 17, 2100 Copenhagen Ø, Denmark

(Dated: October 31, 2018)

We study experimentally superradiant Rayleigh scattering from a Bose-Einstein condensate (BEC) in a new parameter regime where pump depletion and the exchange of photons between the endfire modes are important. Through experiments and simulations we show that collective atom light coupling leads to the self-organized formation of dynamic Bragg gratings within the sample. These gratings lead to an efficient back-scattering of pump photons and optical resonator structures within the BEC.

PACS numbers: 03.75.Nt,37.10.Vz,42.50.Gy

With its extremely high optical depth and unique coherence properties, a Bose Einstein condensate provides an ideal object on which to study collective light scattering with the goal of generating and probing light-atom correlations. Superradiant light scattering (SLS) from ultra-cold atomic ensembles has been recognized as a method to generate entangled atoms and photons due to the fact that the interaction Hamiltonian has the generic form of a parametric amplifier $H \propto \hat{a}^\dagger \hat{b}^\dagger$, where correlations based on momentum conservation arise in the case of Rayleigh scattering [1], and angular momentum in the case of Raman processes [2]. Entanglement in the ultra-low gain regime of such an interaction, when far less than one atom-photon excitation pair is generated on average, forms the basis for a quantum repeater [3] and has been studied extensively [4]. Here, we are interested in the high gain - superradiant - regime where the detection of entanglement requires in general the measurement of both the phase and amplitude of the light and matter waves at the sub-shot noise level. While this is typically hampered by the lack of an atomic analogue to homodyne detection of light, a recent proposal claims entanglement may be detected by just counting photons and atoms [5]. Nonetheless, the full dynamics of coupled matter and light waves where one does not place limitations on the depletion of either the condensate or input light, and where propagation effects are considered, remain important issues if such correlations and entanglement are to be made useful resources.

To this end, we explore superradiant Rayleigh scattering from a trapped, cigar shaped BEC as the pump detuning is varied while the single particle scattering rate R is kept constant. In this way, we investigate the effect of the detuning of the pump beam in the process, and move between the case where the pump beam remains essentially undepleted by the scattering, to the situation where superradiant scattering is ‘clamped’ by a lack of photons in the pump beam. Crucial to these dynamics is the structure that builds up along the long axis of the condensate, demonstrating characteristics from ‘Dicke’ superradiance from extended samples [6, 7, 8], a fact recognized recently both experimentally [9, 10] and theoretically [11, 12, 13, 14]. Contrary to most earlier experimental work on the subject [9, 15, 16, 17], we end-pump along

the long axis with a beam mode-matched to the transverse cross-section of the BEC in order to optimize the coupling between pump photons and atoms. As opposed to the study in [18], which also probed the BEC along its long axis, we use the back-scattered light to monitor the superradiant dynamics with very good time resolution. In view of our ultimate goal to probe light-atom correlations, we have performed a careful calibration of the detection system. As a consequence, we find quantitative agreement with simulations of a 1D semiclassical model over a wide parameter range. The quality of the agreement with experiment supports the use of the simulations to understand the spatial and temporal dynamics inside the sample.

Like superradiance (SR) in electronically inverted samples [19], superradiant light scattering from an ultra-cold atomic sample is a process whereby an initially unoccupied electromagnetic field mode becomes weakly populated through spontaneous emission; these modes are then amplified with the highest gain along the direction of greatest optical depth. In the end-pumped geometry (see Fig. 1), photons are absorbed from the forward travelling beam E_+ and scattered into the backward travelling beam E_- , leading to a concomitant change in the scattered atom’s momentum of $2\hbar k_l$ and a recoil shift in the back-scattered light of four times the recoil frequency ω_r . The forward and backward travelling light waves interfere to give a moving intensity grating with a spatial period of $\lambda/2$ that varies in visibility and phase over the length of the sample. In the case of Rayleigh scattering, the internal ground state of the atom does not change in the process, leading to a density modulation due to interference between the different momentum orders that has the same period as the light intensity modulation. Thus, the physical picture is one of four wave-mixing.

In our experiments, superradiant Rayleigh scattering was induced in a trapped BEC by illuminating it with a pulse of off-resonant light along the long axis of the condensate, as shown in Fig. 1. The BEC was generated by evaporatively cooling a cloud of ^{87}Rb atoms in the $|F = 1, m_F = -1\rangle$ hyperfine state in a Ioffe-Pritchard magnetic trap. We obtain cigar shaped condensates containing 1.35×10^6 atoms, with in-trap Thomas Fermi radii of $r_\perp = 6.4$ and $r_\parallel = 65 \mu\text{m}$ in the radial and axial directions and with no discernible thermal fraction. The pump light was detuned by a variable amount from the $|F = 1, m_F = -1\rangle \rightarrow |F = 2, m_F = -2\rangle$

*hilliard@nbi.dk

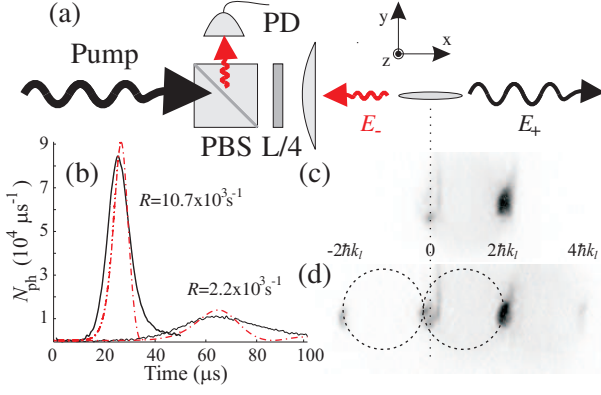


FIG. 1: (Color online) (a) The BEC was end-pumped by a focused, circularly polarized laser beam, and the back-scattered light was directed through a quarter wave plate (L/4) and polarizing beam-splitter (PBS) onto a sensitive photodetector (PD). (b) Traces from PD are shown for low and high pump powers at a detuning of $\delta = -2\pi \times 2.6$ GHz. Simulations for the same parameters are presented as red dash-dot lines. Absorption images after 45 ms time of flight (TOF) of the corresponding atomic distributions are shown in (c) (low power, pump pulse duration 200 μs) and (d) (high power, pump pulse duration 50 μs). Circles indicating the separation of adjacent momentum orders after 45 ms TOF are shown in (d); note that they originate from the input light end ($x = 0$) of the BEC.

transition on the D1 line of ^{87}Rb at 795 nm, and circularly polarized with respect to the long axis of the trap. All data presented is for red detunings ($\delta = \omega_l - \omega_0 < 0$); rectangular pump pulse envelopes; and where the atoms were interrogated in-trap, with the trapping potential extinguished immediately after the end of the pump pulse. The beam was focused to a waist of 13 μm at the center of the condensate with negligible change of beam size over the length of the BEC. Light was back-scattered by the sample in the same polarization as the input beam, and thus the backward travelling light was reflected by the polarizing beamsplitter, then directed onto a sensitive PIN diode photodetector. The detector, with a bandwidth of 400 kHz, is shot-noise limited for photon fluxes greater than $10^5 \mu\text{s}^{-1}$. To avoid back reflections from optics and cell windows that seed the process, the pump beam was inserted at a slight angle (less than 2°). Pictures of the atoms were obtained after 45 ms time of flight by resonant absorption imaging. Figure 1(b) shows experimental and simulated time traces for high and low pump powers, with the corresponding atomic distributions shown in Fig. 1(c) and (d). For single particle scattering rates much smaller than the recoil frequency $\omega_r = 2\pi \times 3.6$ kHz, scattering to higher atomic momentum orders occurs sequentially on a time scale $\sim \tau_r = 2\pi/\omega_r$. Figure 1(c) shows this case, where the transfer is limited to the first order. When $R \sim \omega_r$, there is sufficient gain for atoms to be back-scattered into negative momentum orders, i.e., the Kapitza-Dirac regime where atoms absorb back-scattered light and re-emit into the forward direction, as is evident in Fig. 1(d). An asymmetry in distance between forward and backward scattered atoms and the center of the original condensate after time of flight, observed previously in [9, 11], is visible in Fig. 1(d). This asymmetry can be traced back to the spatial inhomogeneity of superradi-

ant scattering favoring the input end of the condensate, where the amplitude of the reflected light E_- is highest. The spatial dimensions of the condensate and the slow expansion upon release from the trap along the long axis are such that this spatial feature of the scattering is evident after 45 ms time of flight. The momentum distributions are somewhat distorted due to the input angle of the beam: when the beam is aligned parallel to the long axis of the BEC, the Bragg condition is satisfied for the atoms centered around zero transverse momentum, but at the slight incident angle used, the patterns become more complicated. Nevertheless, the arrival times and amplitudes of the first superradiant light pulses are very well described by the simulations.

The dynamics are simulated by numerically solving 1D Maxwell-Schrödinger equations for the evolution of the atomic wavefunctions and the incident and generated light fields [6, 20]. The situation of SLS from a BEC was derived in [11, 12], and we follow closely their notation. In the end-pumped geometry, the Maxwell-Schrödinger equations read:

$$i \frac{\partial \psi_m(\xi, \tau)}{\partial \tau} = -\frac{1}{2} \frac{\partial^2 \psi_m(\xi, \tau)}{\partial \xi^2} - im \frac{\partial \psi_m(\xi, \tau)}{\partial \xi} + \Lambda e_-^*(\xi, \tau) e_+(\xi, \tau) \psi_{m-2}(\xi, \tau) e^{2i(m-1)\tau} + \Lambda e_+^*(\xi, \tau) e_-(\xi, \tau) \psi_{m+2}(\xi, \tau) e^{-2i(m+1)\tau} + \Lambda (|e_+(\xi, \tau)|^2 + |e_-(\xi, \tau)|^2) \psi_m(\xi, \tau), \quad (1)$$

$$\frac{\partial e_+(\xi, \tau)}{\partial \xi} = -i\Lambda \sum_{m=2n} e_-(\xi, \tau) e^{-2i(m-1)\tau} \times \psi_m(\xi, \tau) \psi_{m-2}^*(\xi, \tau) + e_+(\xi, \tau) |\psi_m(\xi, \tau)|^2, \quad (2)$$

$$\frac{\partial e_-(\xi, \tau)}{\partial \xi} = +i\Lambda \sum_{m=2n} e_+(\xi, \tau) e^{2i(m+1)\tau} \times \psi_m(\xi, \tau) \psi_{m+2}^*(\xi, \tau) + e_-(\xi, \tau) |\psi_m(\xi, \tau)|^2, \quad (3)$$

such that $\psi(x, t) = \sum_m \psi_m(x, t) e^{-i(\omega_m t - m k_l x)}$ is the slowly varying 1D wavefunction of momentum order $m = 2n$ for integer n , with $\omega_m = m^2 \omega_r$; and the electric field (suppressing polarization) is given by $E = E_+(x, t) e^{-i(\omega_l t - k_l x)} + E_-(x, t) e^{-i(\omega_l t + k_l x)} + h.c.$; where $E_{\pm}(x, t)$ are slowly varying envelopes. The light fields are scaled such that $E_{\pm} = e_{\pm} \sqrt{\hbar \omega_r k_l / \epsilon_0 A}$; and the scaled space and time variables are related to real space parameters by $\xi = k_l x$ and $\tau = 2\omega_r t$. The coupling constant describing the strength of the interaction is given by $\Lambda = 1/4 \cdot \Gamma / \delta \cdot \sigma_0 / A$, where Γ denotes the linewidth of the optical transition, σ_0 the resonant atomic absorption cross section, and A the cross section of the interaction region. Retardation effects have been neglected in Eqns. (2) and (3) given the length of the condensate $2r_{\parallel} = 130 \mu\text{m}$, which allows us to discard a time derivative term. In this approximation, these equations can be considered as describing the self-consistent light field distribution in a continuous array of Bragg gratings formed by the density modulation of the matter wave. In this 1D model, the endfire mode described

by e_+ and the pump mode coincide. A 1D treatment of the problem is supported by the fact that the Fresnel number of the condensate is of order one, which suggests that the emission of light is predominantly into a single transverse mode [21]. The harmonic trapping potential and the mean field interaction term describing collisions between atoms have been omitted, because they have a limited effect on the focus of these experiments - the first superradiant pulse [22].

Equations (1), (2) and (3) describe a Raman interaction where a ladder of momentum states is coupled by two counter-propagating light fields. It is terms three and four that dominate in Eqn. (1): these describe the local coupling to the nearest momentum states via exchange of photons between e_+ and e_- . The final terms in Eqn. (1) account for phase rotation of the matter wave due to the light shift. Equations (2) and (3) show terms equivalent to the coupling terms in Eqn. (1). Specifically, the growth of e_- occurs with the corresponding growth of recoiling atoms ψ_{m+2} and the decrease of e_+ photons and ψ_m atoms. The last terms in Eqns. (2) and (3) describe the effect on the light of the slowly varying refractive index due to the large scale atomic density distribution.

To compare experimental results with simulations, the equations (1), (2) and (3) were solved numerically for experimental parameters. The initial wavefunction ψ_0 was taken to be a 1D Thomas-Fermi profile normalized to the number of atoms in the trap N_{at} . The boundary conditions for the light fields were typically taken to be $e_+(0, \tau) = e_i$ and $e_-(k_l L, \tau) = 0$. Note that $|e_-(0, \tau)|^2$ is proportional to the back-scattered light intensity measured in experiment, and that the total photon flux is conserved: $|e_+(0, \tau)|^2 = |e_-(0, \tau)|^2 + |e_+(k_l L, \tau)|^2$. As Eqns. (1), (2) and (3) contain no explicit noise term to instigate superradiant scattering, we seed the process by taking a non-zero first order momentum component $\psi_2 = \psi_0 / \sqrt{N_{\text{at}}}$, corresponding to a single delocalized atom in the first side-mode [12]. The random nature of the initiation of superradiant scattering may be modeled in the present formalism by using random initial conditions but here we focus on the large scale dynamics of the system rather than its noise properties [20].

Figure 2(a) shows, for both experimental data (symbols) and simulations (lines), the peak values of the first superradiant pulse as the detuning of the pump beam was varied while keeping the single particle scattering rate R constant. Results are shown for four values of R in the range $R \ll \omega_r$ to $R \sim \omega_r$. For a large portion of the graph, the peak value is essentially independent of the detuning, and there is excellent agreement between simulations and data. The input powers in the simulations have been scaled up by a common factor of 22% [23]. For lower detunings, the peak value of the emitted pulse falls away, and the experimental data reaches our detection resolution for $\delta \approx -2\pi \times 300$ MHz, while the simulations show the same qualitative behaviour.

To further study the two regimes, Fig. 2(b) shows experimental time traces for several different values of R at a high detuning, and Fig. 2(c) shows experimental traces for four low detunings while R is kept constant. Figure 2(b) confirms the qualitative features evident in Fig. 1(b): in the high detuning regime, the superradiant peaks arrive earlier and are more

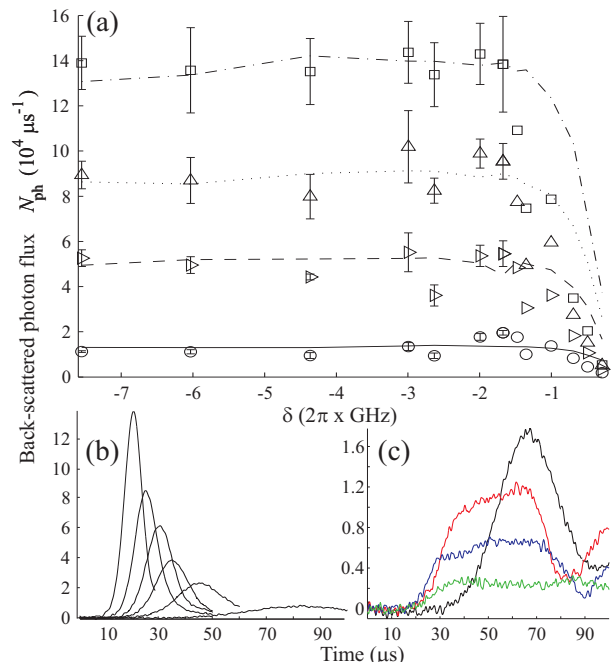


FIG. 2: (Color online) (a) Experimental (symbols) and simulated (lines) peak photon flux of the first superradiant pulse as a function of detuning for $R = 2.2$ (circles, solid line), 6.4 (right triangles, dashed line), 10.7 (upward triangles, dotted line), 15.9 (squares, dash-dot line) $\times 10^3 \text{ s}^{-1}$. Errorbar limits are the standard error of the mean of 5 realizations, and for clarity are omitted in the low detuning portion of the graph. (b) Traces corresponding to the flat portion of Fig. 2(a). The detuning was $\delta = -2\pi \times 2.6$ GHz, for $R = 2.2, 4.3, 6.4, 8.6, 10.7, 15.9 \times 10^3 \text{ s}^{-1}$. For clarity, the traces are edited to show only the first pulse. (c) Traces corresponding to the decaying portion in Fig. 2(a). For $R = 2.2 \times 10^3 \text{ s}^{-1}$ and detunings $\delta = -2\pi \times 2.0$ (black), 1.0 (red), 0.7 (blue), 0.5 (green) GHz.

sharply peaked the higher the pump power. Simple models of superradiance predict a pulse height proportional to R and a pulse delay inversely proportional to R [7], while we observe a faster increase of the peak power and a slower decrease in pulse delay both experimentally and in the simulations. Figure 2(c) shows how the superradiant pulse intensity is clamped at low detunings. The lower amplitudes can be traced back to the lower incident photon fluxes and increasingly important pump depletion in the low detuning case. The transition from high detuning behaviour to the pump-depletion regime occurs in the experimental data at points where the incident photon flux is approximately 10 times the peak reflected photon flux. Above this point, while the amplitude of the reflected pulses drops, the observed peak reflectivity of the sample increases sharply, up to values of $\sim 30\%$. The simulations show the same qualitative behaviour in this regime, and we attribute the loss of quantitative agreement to the incoherent losses that are not captured by the model: i.e., emission into different modes. The spatial dependence of the light and matter waves plays a critical role here, and to gain more insight into the behavior of the system, we explore the light and matter wave dynamics inside the sample through simulations.

Figure 3 shows the results of simulations for the lowest pump power case for high (left side) and low (right side)

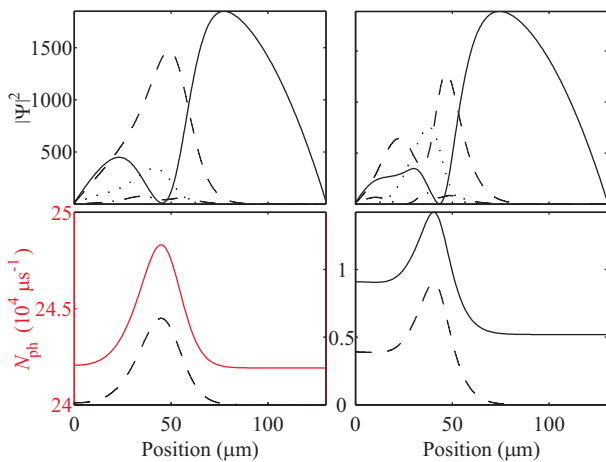


FIG. 3: (Color online) Snapshots of system dynamics inside the sample for high detuning $\delta = -2\pi \times 2$ GHz ((a) and (c)) and low detuning $\delta = -2\pi \times 294$ MHz ((b) and (d)) at the same rate $R = 2.2 \times 10^3 \text{ s}^{-1}$ after an interaction time $t = 87 \mu\text{s}$. (a) and (b) show atomic densities in the momentum modes: $|\psi_{-2}|^2$ (dash-dot line), $|\psi_0|^2$ (solid line), $|\psi_2|^2$ (dashed line), $|\psi_4|^2$ (dotted line). (c) and (d) display light flux ($\propto |e_{\pm}|^2$) within the sample for pump light e_+ (solid lines; in (c), red line and left axis) and reflected light e_- (dashed lines; right scale in (c)). Note the shared scale of e_- in (c) and both e_+ and e_- in (d).

pump detuning, after $87 \mu\text{s}$ of interaction time with the pump beam. Along the long axis of the BEC, atomic distributions are shown in the upper row ((a) and (b)), and the scaled intensities $\propto |e_+|^2$ and $|e_-|^2$ in the lower row ((c) and (d)). The general dynamics for low input power, high detuning are as follows: The back-scattered light intensity in the sample builds up at the input end because there it sees gain from approximately the entire length of the BEC. At this point, atoms are transferred from ψ_0 to ψ_2 concurrently with the growth of e_- and reduction in e_+ . When the population in ψ_0 is sufficiently depleted at the input edge of the BEC, the process slows down, and the light field envelopes move towards the centre of the condensate, where $|\psi_0|$ is still large, and the exchange between the two light fields continues; this is the time shown in Fig. 3. At this time, $|\psi_0|$ grows again at the input end of the condensate, driven there by the destruction of e_- photons generated further inside the sample, and ψ_2 atoms. In this way, the back-scattered photon flux out the input end of the condensate stops, and the first superradiant pulse has been emitted. The basis of ‘ringing’ behaviour - the emission of subsequent SR pulses - is merely a repetition of the dynam-

ics described above. Furthermore, a fascinating implication of the above dynamics, visible in Fig. 3 (c) and (d), is that at times the light intensity within the BEC is higher than outside - the interaction leads to the formation of an optical resonator, where partially reflecting mirrors are formed by the density modulation due to the interference of stationary and recoiling matter-waves. These Bragg gratings are centered where ψ_0 and ψ_2 cross.

The dynamics in the low detuning case is similar, but with two significant differences. Due to the increased light scattering cross-section at low detunings, the pump light is significantly depleted in its passage through the BEC, as is evident in Fig. 3(d). Accordingly, the build up of back-scattered light is even more localized at the input end of the BEC, and the scattering of ψ_0 to ψ_2 atoms is limited to a very narrow region of atoms. This narrowness is reflected at later times in the length of the ‘resonator’, as is evident in Fig. 3(b). Thus, the spatial dependence of the pump depletion and hence the size of the scattering region leads to the reduced amplitude of the back-scattered pulses in Fig. 2. The second main difference is that the ψ_4 mode becomes significantly populated at low detunings, as can be seen in Fig. 3(b). This means that the first SR pulse is not stopped by a lack of ψ_0 atoms, but rather can continue due to the scattering from ψ_2 to ψ_4 via the destruction of a pump photon. This can be seen in Fig. 3(d), where there is more light ‘leaking’ from the resonator compared to Fig. 3(c); and in Fig. 2(c), where the low detuning pulses are broader, and show a secondary peak soon after the first. In general, the dynamics become complicated as the number of significantly atomic orders and hence number of timescales in the problem ($\propto 1/\omega_m$) increases.

In summary, we have studied superradiant scattering of light by Bose condensed atomic samples in new parameter regimes and find very good agreement between experimentally detected light pulses and simulations. The simulations take into account the build-up of longitudinal spatial structure inside the sample of both the light and matter waves. The results help to identify a suitable parameter regime for the experimental study of correlations between light and atoms that arise from superradiance.

Acknowledgments

A. Hilliard would like to thank D. Witthaut for his help with the simulations. This work is supported by the DGF center QUANTOP and EU-projects EMALI and QAP.

[1] M. M. Cola, M. G. A. Paris, and N. Piovella, Phys. Rev. A **70**, 043809 (2004).
 [2] M. G. Moore and P. Meystre, Phys. Rev. Lett. **85**, 5026 (2000).
 [3] L.-M. Duan, M. D. Lukin, J. I. Cirac, and P. Zoller, Nature (London) **414**, 413 (2001).
 [4] H. Kimble, Nature (London) **453**, 1023 (2008).
 [5] C. A. Muschik, E. S. Polzik, and J. I. Cirac, arXiv:0806.3448 (2008).

[6] J. C. MacGillivray and M. S. Feld, Phys. Rev. A **14**, 1169 (1976).
 [7] M. Gross and S. Haroche, Physics Reports **93**, 301 (1982).
 [8] V. V. Zheleznyakov, V. V. Kocharovskiy, and V. Kocharovskiy, Sov. Phys. Usp. **32**, 835 (1989).
 [9] D. Schneble, Y. Torii, M. Boyd, E. W. Streed, D. E. Pritchard, and W. Ketterle, Science **300**, 475 (2003).
 [10] L. E. Sadler, J. M. Higbie, S. R. Leslie, M. Vengalattore, and

- D. M. Stamper-Kurn, Phys. Rev. Lett. **98**, 110401 (2007).
- [11] O. Zobay and G. M. Nikolopoulos, Phys. Rev. A **72**, 041604(R) (2005).
- [12] O. Zobay and G. M. Nikolopoulos, Phys. Rev. A **73**, 013620 (2006).
- [13] H. Uys and P. Meystre, Phys. Rev. A **75**, 033805 (2007).
- [14] Y. A. Avetisyan and E. D. Trifonov, Zh. Eksp. Teor. Fiz. **130**, 771 (2006).
- [15] S. Inouye, A. P. Chikkatur, D. M. Stamper-Kurn, J. Stenger, D. E. Pritchard, and W. Ketterle, Science **285**, 571 (1999).
- [16] D. Schneble, G. K. Campbell, E. W. Streed, M. Boyd, D. E. Pritchard, and W. Ketterle, Phys. Rev. A **69**, 041601(R) (2004).
- [17] Y. Yoshikawa, T. Sugiura, Y. Torii, and T. Kuga, Phys. Rev. A **69**, 041603(R) (2004).
- [18] J. Li, X. Zhou, F. Yang, and X. Chen, Phys. Lett. A **372**, 4750 (2008).
- [19] R. H. Dicke, Phys. Rev. **93**, 99 (1954).
- [20] F. Haake, H. King, G. Schröder, J. Haus, and R. Glauber, Phys. Rev. A **20**, 2047 (1979).
- [21] N. E. Rehler and J. H. Eberly, Phys. Rev. A **3**, 1735 (1971).
- [22] While a BEC is not a prerequisite for superradiant scattering, it allows us here to neglect dephasing of density modulations due to thermal atomic motion.
- [23] The main source of uncertainty in the coupling strength is the geometrical overlap between beam and BEC.